IVYSPRING INTERNATIONAL PUBLISHER

Theranostics

2016; 6(1): 93-103. doi: 10.7150/thno.12766

Research Paper

Feasibility of Affibody Molecule-Based PNA-Mediated Radionuclide Pretargeting of Malignant Tumors

Hadis Honarvar[1*], Kristina Westerlund[2*], Mohamed Altai[1], Mattias Sandström[3], Anna Orlova[4], Vladimir Tolmachev[1#], Amelie Eriksson Karlström[2#✉]

1. Department of Immunology, Genetics and Pathology, Uppsala University, Uppsala, Sweden
2. School of Biotechnology, Division of Protein Technology, KTH Royal Institute of Technology, Stockholm, Sweden
3. Section of Nuclear Medicine and PET, Department of Surgical Sciences, Uppsala University, Uppsala, Sweden
4. Preclinical PET Platform, Department of Medicinal Chemistry, Uppsala University, Uppsala, Sweden

*These authors contributed equally

Shared senior authorship

✉ Corresponding author: Prof. Amelie Eriksson Karlström, School of Biotechnology, Division of Protein Technology, KTH Royal Institute of Technology, AlbaNova University Center, 106 91 Stockholm, Sweden. Phone: +46 8 5537 8333; Fax: +46 8 5537 8481; E-mail: amelie@biotech.kth.se

Received: 2015.05.22; Accepted: 2015.09.18; Published: 2016.01.01

Abstract

Affibody molecules are small (7 kDa), non-immunoglobulin scaffold proteins with a potential as targeting agents for radionuclide imaging of cancer. However, high renal re-absorption of Affibody molecules prevents their use for radionuclide therapy with residualizing radiometals. We hypothesized that the use of Affibody-based peptide nucleic acid (PNA)-mediated pretargeting would enable higher accumulation of radiometals in tumors than in kidneys. To test this hypothesis, we designed an Affibody-PNA chimera $Z_{HER2:342}$-SR-*HP1* containing a 15-mer *HP1* PNA recognition tag and a complementary *HP2* hybridization probe permitting labeling with both ^{125}I and ^{111}In. ^{111}In-$Z_{HER2:342}$-SR-*HP1* bound specifically to HER2-expressing BT474 and SKOV-3 cancer cells in vitro, with a K_D of 6±2 pM for binding to SKOV-3 cells. Specific high affinity binding of the radiolabeled complementary PNA probe ^{111}In-/^{125}I-*HP2* to $Z_{HER2:342}$-SR-*HP1* pre-treated cells was demonstrated. ^{111}In-$Z_{HER2:342}$-SR-*HP1* demonstrated specific accumulation in SKOV-3 xenografts in BALB/C nu/nu mice and rapid clearance from blood. Pre-saturation of SKOV-3 with non-labeled anti-HER2 Affibody or the use of HER2-negative Ramos xenografts resulted in significantly lower tumor uptake of ^{111}In-$Z_{HER2:342}$-SR-*HP1*. The complementary PNA probe ^{111}In/^{125}I-*HP2* accumulated in SKOV-3 xenografts when $Z_{HER2:342}$-SR-*HP1* was injected 4 h earlier. The tumor accumulation of ^{111}In/^{125}I-*HP2* was negligible without $Z_{HER2:342}$-SR-*HP1* pre-injection. The uptake of ^{111}In-*HP2* in SKOV-3 xenografts was 19±2 %ID/g at 1 h after injection. The uptake in blood and kidneys was approximately 50- and 2-fold lower, respectively. In conclusion, we have shown that the use of Affibody-based PNA-mediated pretargeting enables specific delivery of radiometals to tumors and provides higher radiometal concentration in tumors than in kidneys.

Key words: Affibody, peptide nucleic acid, radionuclide pretargeting, scaffold protein, HER2

Introduction

The use of monoclonal antibodies (mAbs) for therapy improves the survival of patients with disseminated cancer. However, the antibody treatment is rather cytostatic than cytotoxic and in addition, many tumors develop a resistance to antibody therapy. Conjugation of mAbs with cytotoxic drugs or radionuclides increases their therapeutic potential. The use of radionuclides as cytotoxic payload offers the advantage of "cross-fire" effect, when particles emitted by nuclides specifically delivered to cancer cells irradiate other surrounding cancer cells (1). Therefore, it is unnecessary to deliver radionuclides to every ma-

lignant cell in a cluster. Clinical mAb-mediated radionuclide therapy (radioimmunotherapy, RIT) has demonstrated a high potential for treatment of radiosensitive hematologic malignancies, but has failed to improve the survival of patients with solid tumors (2). Several biodistribution features of whole-length mAbs contributed to the failure to deliver sufficient dose to the tumors without damaging healthy tissues, e.g. long residence time in circulation, poor extravasation and limited penetration into tumor mass. These features are to a high extent determined by the large size of mAbs.

One approach to overcome problems of RIT is pretargeting. In this case, a mAb fitted with a recognition tag is injected first. After mAb localization in the tumor and its clearance from blood and other non-targeted compartments, a radiolabeled secondary agent, which can bind specifically to a recognition tag, is injected. The secondary agent is typically smaller, which provides rapid extravasation and localization in tumors, as well as a rapid clearance from blood. Proof-of-concept of pretargeting was demonstrated using an avidin-biotin system for secondary recognition (3–4). The major issue with this system was the immunogenicity of (strept)avidin (4) and interference with endogenous biotin (5). To overcome this, a number of alternative approaches to secondary recognition have been developed. Examples are the development of bispecific antibodies, with one of the arms being specific to a small radiolabeled hapten (6), the use of interactions of complementary oligonucleotides or their analogues (7–9), and the use of bioorthogonal chemistry, e.g. the reaction between trans-cyclooctene and electron-deficient tetrazines (10).

In this study, we evaluated pretargeting using Affibody molecules as targeting agents. Affibody molecules are small (7 kDa), non-immunoglobulin scaffold proteins that can be selected to bind with high affinity to cancer-associated molecular targets (11). Numerous preclinical studies demonstrated that Affibody molecules can efficiently and specifically image tumor xenografts in vivo (12). The radiolabeled Affibody molecule ABY-025 has demonstrated specific high-contrast imaging of HER2-expressing tumors in clinical studies (13). Clinical studies suggest that Affibody molecules are non-toxic and non-immunogenic. However, the renal clearance of Affibody molecules is accompanied by nearly quantitative reabsorption and rapid internalization in proximal tubuli. In the case of residualizing labels, this causes radioactivity accumulation in kidneys that is several-fold higher than the accumulation in tumors. This prevents the use of such promising therapeutic radionuclides as the low-energy beta emitters ^{177}Lu or ^{161}Tb for Affibody-mediated therapy. Nevertheless, features of the Affibody molecules such as very slow internalization (20-30% after incubation during 24 h) and rapid blood clearance (14) make them attractive as primary targeting agents in pretargeting.

In this study, we evaluated an Affibody-based pretargeting mediated by peptide nucleic acid (PNA) interaction with complementary PNA (Figure 1 B). In a DNA polymer, the backbone is made up of repeating deoxyribose-phosphate groups whereas PNA has a pseudopeptide backbone made up of N-(2-aminoethyl)-glycine units connected through amide bonds (Figure 1 A). PNA is capable of selective and high affinity hybridization to a complementary PNA strand obeying the Watson-Crick hydrogen-bonding rules (15). Importantly, PNA is non-immunogenic and non-toxic (16–18). In addition, PNA is not degraded in vivo by peptidases or nucleases, as it is neither a regular peptide, nor a nucleic acid. Earlier studies (8, 19–20) have demonstrated the feasibility of PNA-PNA-hybridization in vivo. It has to be noted, that in these studies PNA-conjugated beads instead of tumors were used as models, or non-specific accumulation of avidin-PNA in tumors and inflammation sites were used, to deliver non-labeled PNA to areas of interests. Strictly speaking, true molecular target-specific PNA-mediated pretargeting has not been shown.

The aim of this study was to provide a proof-of-principle for Affibody-based PNA-mediated pretargeting. The main hypotheses were that i) an Affibody-PNA chimera can specifically localize in tumors, ii) Affibody-based PNA-mediated pretargeting provides specific accumulation of radiolabeled PNA in tumors, and iii) Affibody-based PNA-mediated pretargeting can provide higher accumulation of radiometals in tumors in comparison to kidneys. To test these hypotheses, two complementary PNA-based hybridization probes, *HP1* and *HP2*, were designed (Figure 1 C). *HP1* has a three-glycine motif in the N-terminal and was designed to be covalently attached to a recombinantly expressed Affibody molecule, $Z_{HER2:342}$-SR-H_6 (Figure 1 C), via sortase A mediated ligation. A versatile DOTA chelator was introduced in the design of *HP1*, and is thus present in the Affibody-PNA chimera $Z_{HER2:342}$-SR-*HP1* (Figure 1 C). The chelator could be labeled with ^{111}In or ^{68}Ga for pretreatment monitoring of $Z_{HER2:342}$-SR-*HP1* accumulation in tumors using SPECT or PET, respectively. This theranostic approach enables selection of patients, which accumulate sufficient amount of primary probe in tumors and would most likely respond to Affibody-based pretargeted therapy. The secondary hybridization probe *HP2* was conjugated with both a

DOTA chelator and a tyrosine. The use of DOTA enables labeling with a broad range of radiometals suitable for therapeutic applications, such as ^{177}Lu, ^{47}Sc, ^{161}Tb, ^{212}Bi, ^{213}Bi, and ^{227}Th. The introduction of tyrosine makes labeling with a therapeutic radiohalogen, ^{131}I, possible. In this proof-of-principle study, we used surrogate radionuclides, ^{111}In as a radiometal and ^{125}I as a radioiodine.

Materials and Methods

Detailed descriptions of materials, equipment and methods used in this study are, unless otherwise stated, given in the **Supplementary Material.**

Production and purification of hybridization probes, proteins and the Affibody-PNA chimera

A detailed description of materials and methods used for the molecular cloning and expression of recombinant proteins, the synthesis of pretargeting hybridization probes and the sortase A mediated $Z_{HER2:342}$-SR-*HP1* ligation is provided in reference (21).

Cell culture

For in vitro studies, human ovarian cancer SKOV-3 and human breast cancer BT474 cell lines with high (over 10^6 receptors per cell) HER2 expression (22–23) were used. As in vivo models, HER2-positive SKOV-3 ovarian cancer and HER2-negative Ramos lymphoma xenografts were used. All cell lines were from American Type Culture Collection (ATCC). Cells were cultured in RPMI medium (Flow Irvine), supplemented with 10 % fetal calf serum (Sigma), 2 mM L-glutamine, and PEST (penicillin, 100 IU/mL, and streptomycin, 100 mg/mL; Biokrom Kg).

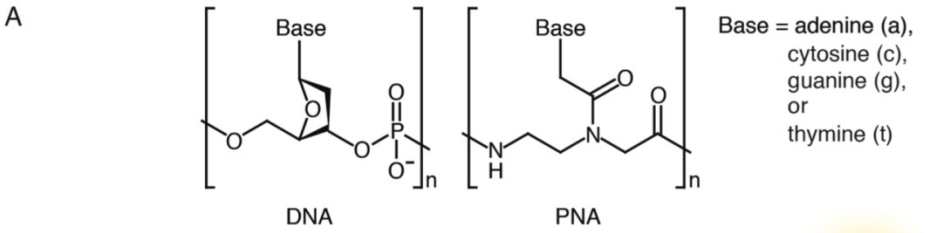

C

Hybridization probes, proteins & conjugates

Name	Sequence
HP1	GGGSS-agt ctg gat gta gtc-EK(DOTA)-[AEEA]-E-NH_2
HP2	DOTA-[AEEA]-SS-gac tac atc cag act-EEY-NH_2
$Z_{HER2:342}$-SR-H_6	•VDNKFNKEMR NAYWEIALLP NLNNQQKRAF IRSLYDDPSQ SANLLAEAKK LNDAQAPK• VDGSGSGSLPET GGHHHHHH
$Z_{HER2:342}$-SR-*HP1*	•VDNKFNKEMR NAYWEIALLP NLNNQQKRAF IRSLYDDPSQ SANLLAEAKK LNDAQAPK• VDGSGSGSLPET GGGSS-agt ctg gat gta gtc-EK(DOTA)-[AEEA]-E-NH_2

DOTA=1,4,7,10-tetraacacyclododecane-1,4,7,10-tetraacetic acid, [AEEA]= [2-(2-aminoethoxy)ethoxy]acetic acid

Figure 1: A) Structure of DNA (left) and PNA (right). In a DNA polymer the backbone is made up of repeating deoxyribose-phosphate groups whereas PNA has a pseudo-peptide backbone made up of N-(2-aminoethyl)-glycine units connected through amide bonds. B) Schematic illustration of two-step Affibody molecule-based PNA-mediated pretargeting in vivo. In step 1 the primary probe, the Affibody-PNA conjugate $Z_{HER2:342}$-SR-*HP1*, is injected and allowed to bind to HER2-overexpressing tumor cells. After a certain time, selected to optimize the tumor-to-normal tissue ratio of $Z_{HER2:342}$-SR-*HP1*, the radiolabeled secondary probe *HP2* is injected in step 2. The 15-mer PNA sequence in *HP2* is complementary to *HP1* and the probe is designed to hybridize to the Affibody-PNA conjugate that has accumulated in the tumor in step 1. C) Sequences of hybridization probes, proteins and conjugates. Amino acids are given in one-letter code (upper-case) and PNA monomers in lower-case letters (a, c, g and t). DOTA and [AEEA] denotes the chelator 1,4,7,10-tetraacacyclododecane-1,4,7,19-tetraacetic acid and the spacer unit [2-(2-aminoethoxy)ethoxy]acetic acid, respectively. The parental sequence of the $Z_{HER2:342}$ Affibody molecule is surrounded by bullets.

In vitro cell binding and processing of radiolabeled $Z_{HER2:342}$-SR-*HP1* and *HP2*

In vitro specificity of ^{111}In-$Z_{HER2:342}$-SR-*HP1* binding to HER2-expressing cells was tested by saturating receptors by addition of a large excess of an anti-HER2 $Z_{HER2:342}$ Affibody molecule (24). Another set of experiments was performed to test if binding of radiolabeled *HP2* to cells is dependent on pre-treatment with $Z_{HER2:342}$-SR-*HP1* and the PNA-PNA interaction. Cells were pre-incubated with $Z_{HER2:342}$-SR-*HP1* for 60 min, washed and radiolabeled *HP2* was added to the cells. After incubation for 60 min, cells were washed, detached by trypsin and cell-associated radioactivity was measured. The following control experiments were performed: cells were treated with a large excess of parental anti-HER2 $Z_{HER2:342}$ Affibody molecule to prevent $Z_{HER2:342}$-SR-*HP1* binding and with a large excess of non-labeled *HP2* to prevent specific binding of radiolabeled *HP2*. Non-specific binding of radiolabeled *HP2* without treatment by $Z_{HER2:342}$-SR-*HP1* was measured. For experimental details see **Supplementary Material**.

In vitro cellular processing of ^{111}In-$Z_{HER2:342}$-SR-*HP1* as well as of ^{111}In-*HP2* by HER2-expressing SKOV-3 and BT474 cells were measured, after interrupted incubation, by the acid wash method (24). Cellular retention of ^{125}I-*HP2* was measured, after interrupted incubation, without discrimination between internalized and membrane-bound activity, as internalization would be underestimated for the non-residualizing radioiodine label. For experimental details see **Supplementary Material**.

Binding affinities of ^{111}In-$Z_{HER2:342}$-SR-*HP1* to HER2-expressing cells and ^{125}I-*HP2* to $Z_{HER2:342}$-SR-*HP1* bound to HER2-expressing cells were measured using LigandTracer Yellow and LigandTracer Gray instruments (Ridgeview Instruments AB, Vänge, Sweden) and analyzed by Interaction Map software (Ridgeview Diagnostics AB, Uppsala, Sweden) as described by Björkelund and co-workers (25). For experimental details see **Supplementary Material**.

In vivo evaluation of radiolabeled *HP2* and $Z_{HER2:342}$-SR-*HP1*

All animal experiments were performed in accordance with national legislation on laboratory animals' protection and have been approved by the ethics committee for Animal Research in Uppsala. Euthanasia was performed under Rompun/Ketalar anesthesia.

A group of 4-6 mice was used for each data point. The mice were euthanized at predetermined time points post injection (p.i.) by overdosing of anesthesia followed by heart puncture and exsanguination. Blood and organ samples were collected and their weight and radioactivity were measured. Organ uptake values were calculated as percent of injected dose per gram of tissue (%ID/g). In the case of the dual label study, the whole spectrum of each sample was recorded. The use of γ-spectroscopy enabled the biodistribution measurement of ^{111}In and ^{125}I in each animal independently (26).

To determine an optimal injection route, biodistribution of ^{111}In-$Z_{HER2:342}$-SR-*HP1* (25 kBq; 1μg/mouse) was measured after intravenous and subcutaneous injection in NMRI mice (average weight 24±1 g) at 1, 4 and 24 h p.i. Earlier studies (27) have demonstrated that biodistribution of monomeric Affibody molecules in mice are nearly identical after intravenous and subcutaneous injection. The use subcutaneous injection of Affibody-PNA chimera might help to avoid two tail vein injections during the same day in pretargeting studies.

In vivo stability of conjugates was evaluated according to the method developed for intact Affibody molecules by Marek-Kramer and co-workers (28). Two NMRI mice were injected with ^{111}In-$Z_{HER2:342}$-SR-*HP1*, ^{111}In-*HP2* or ^{125}I-*HP2* I the tail vein (1 MBq per animal). At 1 h after injections, the animals were euthanized and blood was withdrawn by heart puncture using a heparinized syringe. The samples were centrifuged (4500 g, 10 min, 4 ^{o}C). Radiolabeled probes (high molecular weight) were separated from radiocatabolites (low molecular weight) using NAP-5 columns (5-kDa cut-off) eluted with PBS. Radioactivity of each fraction was measured, and a percentage of radioactivity in high-molecular-weight fraction was calculated.

For establishing HER2-positive xenografts, ca. 10^7 SKOV-3 cells were subcutaneously implanted in the right hind leg in BALB/C nu/nu mice. For HER2-negative controls, ca. $5x10^6$ Ramos cells were subcutaneously implanted. At the time of experiments, the average animal weights were 18±3 g and 19±1 g for mice bearing SKOV-3 and Ramos xenografts, respectively. The average tumor weights were 0.3±0.2 g and 0.28±0.2 g for SKOV-3 and Ramos xenografts, respectively.

Specificity of $Z_{HER2:342}$-SR-*HP1* binding to HER2 in vivo was tested by injection of 5 μg (30 kBq) ^{111}In-$Z_{HER2:342}$-SR-*HP1* in two groups of mice bearing SKOV-3 xenografts and one group bearing HER2-negative Ramos xenografts. One group with HER2-positive SKOV-3 xenografts was co-injected with an excess amount (500 μg) of non-labeled parental $Z_{HER2:342}$ Affibody molecule. The biodistribution was measured at 5 h after injection.

To evaluate the influence of injected probe dose on tumor targeting, a dual label study was performed. Mice were injected with ^{111}In-$Z_{HER2:342}$-SR-*HP1* (20 kBq per mouse). The injected probe dose was adjusted with non-labeled $Z_{HER2:342}$-SR-*HP1* to 5 (two groups), 30 or 100 µg per mouse. At 4 h after injection of $Z_{HER2:342}$-SR-*HP1*, the mice were injected with 1 µg (20 kBq) of ^{125}I-*HP2*. In addition, one group of mice pre-injected with 5 µg $Z_{HER2:342}$-SR-*HP1* was injected with 5 µg ^{125}I-*HP2*. To test if the tumor accumulation of ^{125}I-*HP2* is mediated by $Z_{HER2:342}$-SR-*HP1*, one group of mice was injected with 1 µg (20 kBq) ^{125}I-*HP2* without pre-injection of $Z_{HER2:342}$-SR-*HP1*. All animals were sacrificed and the biodistribution was measured at 1 h after injection of ^{125}I-*HP2*.

To evaluate pretargeting of ^{111}In-*HP2* and test its specificity, two groups of mice were injected with 1 µg (30 kBq) ^{111}In-*HP2*, and the biodistribution was measured at 1 h after injection. One group was pre-injected with 100 µg $Z_{HER2:342}$-SR-*HP1* 4 h before injection of ^{111}In- *HP2*.

Imaging

Imaging was performed to obtain a visual confirmation of ex vivo measurements. Mice bearing SKOV-3 xenografts were used. Four animals were injected with 1 µg of ^{111}In-*HP2*. Two of these mice were pre-injected with100 µg $Z_{HER2:342}$-SR-*HP1* at 4 h before injection of ^{111}In-*HP2*. For comparison, two mice were injected with 2 µg of previously studied ^{111}In-DOTA-$Z_{HER2:K58}$ (29) Affibody molecule. All animals were injected with 650 kBq of the radiolabeled compounds 1 h before the image acquisition. Immediately before imaging (1 h p.i.), the animals were sacrificed by cervical dislocation. A single image of all animals was acquired simultaneously. The imaging experiment was performed using a GE Infinia gamma camera equipped with a medium energy general purpose (MEGP) collimator. Static images (30 min) were obtained with a zoom factor of 3 in a 256×256 matrix.

Results

Preparation of hybridization probes, proteins and the Affibody-PNA chimera

The production of hybridization probes, $Z_{HER2:342}$-SR-H_6 and the $Z_{HER2:342}$-SR-*HP1* chimera is described in detail in a separate paper (21). Briefly, the PNA-based hybridization probes, *HP1* and *HP2*, were successfully assembled using commercially available building blocks and Fmoc-protected solid-phase chemistry according to standard procedures. The bacterial transpeptidase sortase A was used to site-specifically and irreversibly attach *HP1* to a recombinantly expressed anti-HER2 Affibody molecule, $Z_{HER2:342}$-SR-H_6, to produce the Affibody-PNA chimera, $Z_{HER2:342}$-SR-*HP1*. The identity of the hybridization probes and the Affibody-PNA chimera was verified using electrospray mass spectrometry. The final purity of $Z_{HER2:342}$-SR-*HP1* and *HP2*, used for in vitro and in vivo studies, was analyzed with HPLC and estimated to be >90 and >95%, respectively.

Radiolabeling

$Z_{HER2:342}$-SR-*HP1* was labeled with ^{111}In with a yield of 96.8±0.0%. The purity after NAP-5 size-exclusion chromatography purification was 99.2±0.0%. Labeling of *HP2* with ^{111}In provided a yield of 86.6±10.4% and a purity of 96±6% after NAP-5 purification. A challenge with 500-fold excess of EDTA during 4 h confirmed stability of both ^{111}In-labeled conjugates. ^{125}I-iodination of *HP2* resulted in 85±12% yield and 96±6% purity after purification using NAP-5. A stability test revealed no measurable release of radioiodine after 4 h incubation in human serum at 37 °C.

Binding and processing by HER2-expressing SKOV-3 and BT474 cells in vitro

Binding of ^{111}In-$Z_{HER2:342}$-SR-*HP1* to HER2-expressing SKOV-3 and BT474 cells was significantly ($p<0.00005$) reduced by pre-saturation of receptors by non-labeled anti-HER2 Affibody molecule (Figure 2 A and B). In addition, binding to HER2-negative UN-SCC74B cells was 400-fold lower compared to binding to SKOV-3 cells, and could not be saturated (see Supplementary Figure S4). This demonstrates that binding of $Z_{HER2:342}$-SR-*HP1* is HER2-dependent.

Binding of ^{125}I-*HP2* to both HER2-expressing cell lines pre-treated with $Z_{HER2:342}$-SR-*HP1* was significantly ($p<0.00005$) reduced when receptors were blocked with a large excess of parental anti-HER2 Affibody molecules, or when cell-bound $Z_{HER2:342}$-SR-*HP1* was saturated by a large excess of non-labeled *HP2* (Figure 2 C and D). Binding of ^{125}I-*HP2*, i.e. binding without pre-treatment with $Z_{HER2:342}$-SR-*HP1*, was also significantly ($p<0.00005$) lower than with pre-treatment (Figure 2 C and D). The same was true for binding of ^{111}In-*HP2* (Figure 2 E and F). In addition, binding of both ^{125}I-*HP2* and ^{111}In-*HP2* to HER2-negative UN-SCC74B cells pre-treated with $Z_{HER2:342}$-SR-*HP1* was much lower compared to binding to SKOV-3 cells, and could not be saturated (see Supplementary Figure S5). This demonstrated that binding of $Z_{HER2:342}$-SR-*HP1* to cells is dependent on both HER2 and the presence of bound $Z_{HER2:342}$-SR-*HP1*.

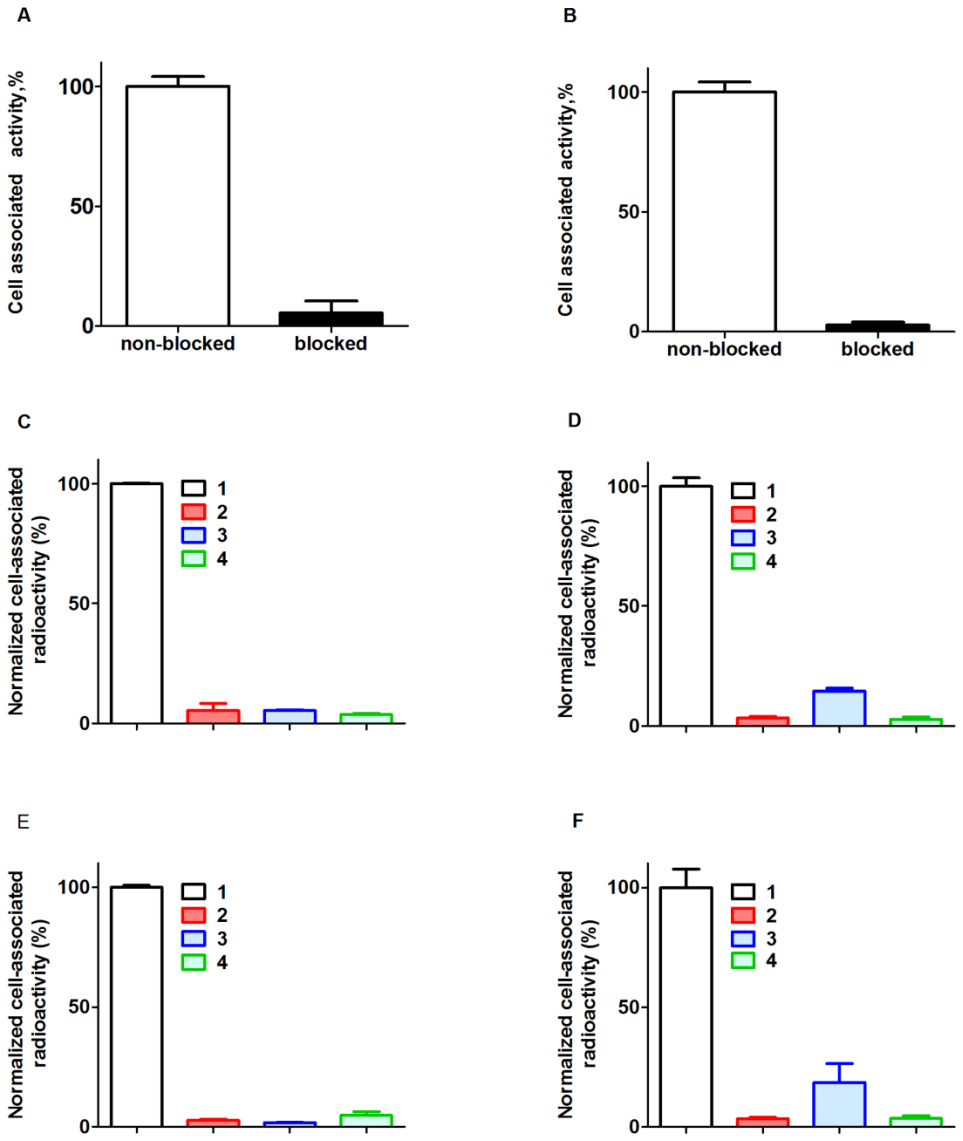

Figure 2. Binding specificity. Binding of ^{111}In-$Z_{HER2:342}$-SR-*HP1* to HER2-expressing cells SKOV-3 (A) and BT474 (B) is saturable. ^{125}I-*HP2* binds to SKOV-3 (C) and BT474 (D) cells pre-treated with $Z_{HER2:342}$-SR-*HP1* (**1**). Saturation of HER2 by large molar excess of non-labeled $Z_{HER2:342}$ (**2**) or saturation of $Z_{HER2:342}$-SR-*HP1* by large molar excess of non-labeled *HP2* (**3**) reduced binding significantly. Binding of ^{125}I-*HP2* without pre-treatment with $Z_{HER2:342}$-SR-*HP1* is significantly lower (**4**) than with pre-treatment. The same is the true for ^{111}In-*HP2* (E and F). Cells were incubated with the labeled compounds at 37 °C. Data are presented as a mean value and standard deviation for three cell culture dishes. Error bars might not be seen in some, because they are smaller than the symbols.

Cellular processing of radiolabeled conjugates by SKOV-3 and BT474 cells after interrupted incubation is presented in Figure 3. The pattern of cellular retention and processing of ^{111}In-$Z_{HER2:342}$-SR-*HP1* was similar for both cell lines. The initial dissociation phase (ca. 4 h) was followed by a plateau at approximately 80% of initially bound radioactivity (Figure 3 A and B). Internalization was relatively slow for ^{111}In-$Z_{HER2:342}$-SR-*HP1*. The internalized fraction at 4 h was 8.0±0.3 % and 11±1% for SKOV-3 and BT474, respectively. At 24 h, the respective values were 24.0±0.7 % and 21±3 %. The processing and retention profile for the ^{111}In-*HP2*: $Z_{HER2:342}$-SR-*HP1* complex was similar to the profile of ^{111}In-$Z_{HER2:342}$-SR-*HP1*, with somewhat higher internalization rate (Figure 3 A and B). The overall cell-associated radioactivity was still approximately 80% of initially bound radioactivity at 24 h. The cellular retention profile of the ^{125}I-*HP2*: $Z_{HER2:342}$-SR-*HP1* complex was different. An initial release was not followed by a plateau, but by a more shallow decrease. The profile of the second descendent segment of the retention curve correlated well with the profile of membrane-bound activity of the ^{111}In-*HP2*:$Z_{HER2:342}$-SR-*HP1* complex. The cellular retention of radioactivity at 24 h was 49±1 % and 40.2±0.4% for SKOV-3 and BT474, respectively.

According to LigandTracer measurements, the equilibrium dissociation constant (K_D) of ^{111}In-$Z_{HER2:342}$-SR-*HP1* binding to SKOV-3 cells was 6±2 pM at both room temperature and 4 °C. The in-

teraction of radiolabeled *HP2* with $Z_{HER2:342}$-SR-*HP1*-treated HER2-expressing cells was best fitted to a 1:2 interaction model, suggesting that the interaction has two dissociation constants: 293±112 pM and 12.8±6 nM for ^{125}I-*HP2*, and 336±13 pM and 15±5 nM for ^{111}In-*HP2* (Figures S6-8).

Animal studies

Comparison of intravenous (iv) and subcutaneous (sc) injection routes of ^{111}In-$Z_{HER2:342}$-SR-*HP1* (Table S1) suggested more rapid blood clearance of ^{111}In-$Z_{HER2:342}$-SR-*HP1* after iv injection in comparison to that after sc injection. Intravenous injection of $Z_{HER2:342}$-SR-*HP1* was selected for further studies.

In vivo stability tests demonstrated that at 1 h after injection, 96.8±0.5%, 98.7±0.2%, 49.7±0.2%, of blood-born radioactivity was associated with ^{111}In-$Z_{HER2:342}$-SR-*HP1*, ^{111}In-*HP2* or ^{125}I-*HP2*, respectively.

Data regarding the specificity of ^{111}In-$Z_{HER2:342}$-SR-*HP1* are presented in Figure 4 A. The uptake in both HER2-negative Ramos (0.16±0.06 %ID/g) and saturated SKOV-3 (0.5±0.1 %ID/g) xenografts was significantly ($p < 0.05$) lower than the uptake in non-saturated SKOV-3 xenografts (8±2%ID/g), demonstrating that tumor targeting was HER2-specific. The difference in biodistribution after injection of 5, 30 and 100 μg ^{111}In-$Z_{HER2:342}$-SR-*HP1* in mice bearing SKOV-3 xenografts was within error of measurements (Figure 4 B).

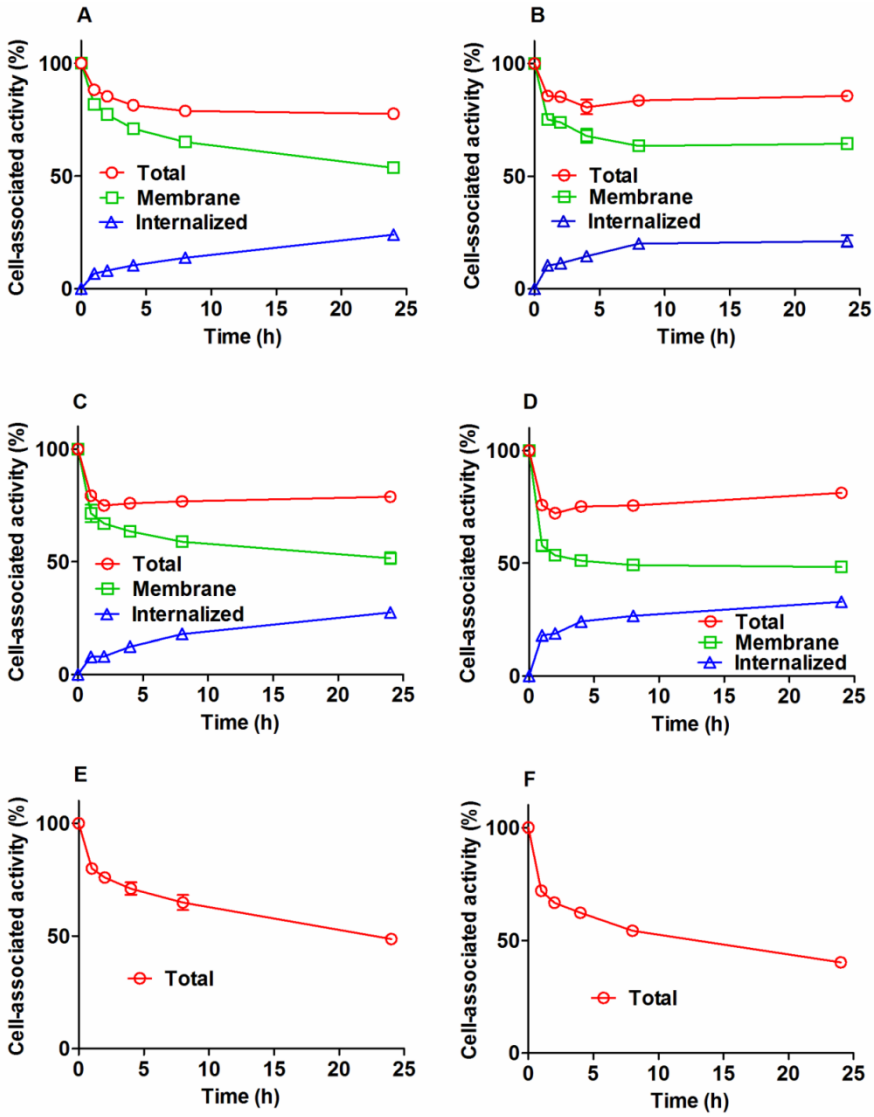

Figure 3. Cellular processing of ^{111}In-$Z_{HER2:342}$-SR-*HP1* (A and B), ^{111}In-*HP2* (C and D), and ^{125}I-*HP2* (E and F), by HER2-expressing SKOV-3 (A, C, and E) and BT474 (B, D and F) cells after interrupted incubation with labeled compounds. In the case of labeled *HP2*, cells were pre-treated with non-labeled $Z_{HER2:342}$-SR-*HP1*. Cells were incubated with the labeled compound at 37 °C. Circles show total cell-associated radioactivity. In the case of radiometals, an acid wash was used to discriminate between the membrane-bound (squares) and internalized (triangles) radioactivity. Data are presented as a mean value and standard deviation for three cell culture dishes. Error bars might be not seen when they are smaller than the symbols.

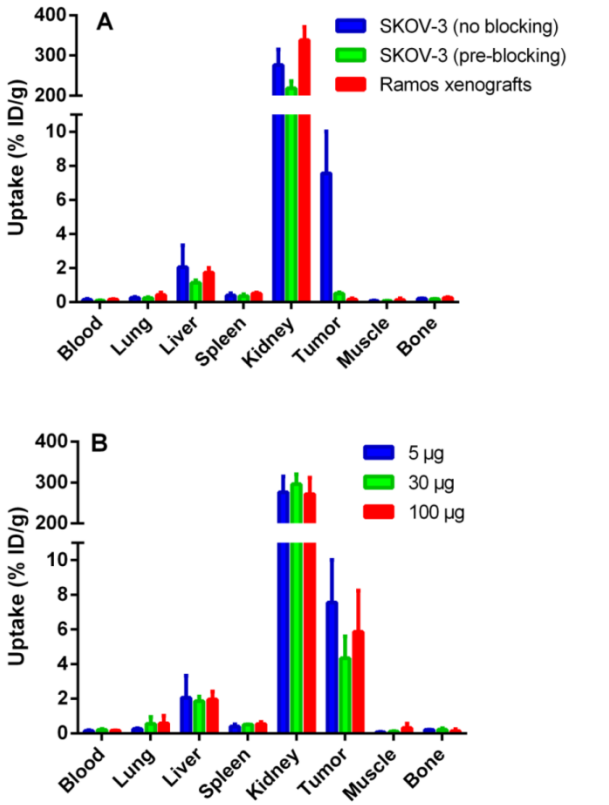

Figure 4. In vivo targeting using ^{111}In-$Z_{HER2:342}$-SR-*HP1* at 5 h p.i., demonstrating the HER2-specificity of ^{111}In-$Z_{HER2:342}$-SR-*HP1* in vivo (A). All animals were injected with 5 µg ^{111}In-$Z_{HER2:342}$-SR-*HP1*. The blocked group with HER2-positive SKOV-3 xenografts was co-injected with an excess amount (500 µg) of non-labeled ZHER2:342 Affibody molecule (green bars). A group with HER2-negative Ramos xenografts was used as a negative control (red bars). Biodistribution in mice bearing SKOV-3 xenografts after injection of 5 (blue bars), 30 (green bars) and 100 (red bars) µg ^{111}In-$Z_{HER2:342}$-SR-*HP1* (B). Data are presented as an average %ID/g with standard deviation for 5 mice.

Pre-injection of $Z_{HER2:342}$-SR-*HP1* at any tested dose provided significantly ($p<0.05$) higher uptake of ^{125}I-*HP2* in SKOV-3 xenografts compared with the uptake of ^{125}I-*HP2* without pre-injection of $Z_{HER2:342}$-SR-*HP1* (Table 1). This indicates that the tumor accumulation of ^{125}I-*HP2* is dependent on the PNA-PNA interaction, i.e. pretargeting. Furthermore, the tumor uptake after injection of 5 µg of ^{125}I-*HP2* was significantly ($p<0.05$) lower than the uptake after injection of 1 µg, when animals were pre-injected with 5 µg of $Z_{HER2:342}$-SR-*HP1*. This demonstrates that the tumor uptake of ^{125}I-*HP2* is saturable.

At the injected ^{125}I-*HP2* dose of 1 µg, the uptake of ^{125}I-*HP2* in tumors was significantly higher than in any organ or tissue including kidneys. The influence of the injected $Z_{HER2:342}$-SR-*HP1* dose on the uptake of ^{125}I-*HP2* was moderate, but the uptake was significantly higher in lung, spleen and kidneys after pre-injection of 100 µg $Z_{HER2:342}$-SR-*HP1* compared with 5 µg. The kidney uptake of ^{125}I-*HP2* after injection of 5 µg was 4-fold higher than after the injection of 1 µg. The tumor-to-blood, -lung, -liver and -spleen ratios were significantly higher for 1 µg injected ^{125}I-*HP2* (Table 1).

The tumor uptake of ^{111}In-*HP2* after pre-injection of $Z_{HER2:342}$-SR-*HP1* (19±2 %ID/g) was significantly ($p<0.05$) higher than the uptake without pre-injection (0.3±0.1 %ID/g) (Table 2). This suggests that the tumor uptake of ^{111}In-*HP2* was dependent on pretargeting. Importantly, the uptake of the radiometal-labeled *HP2* was ca. 2-fold higher in tumors than in kidneys (Table 2).

Table 1. Biodistribution of ^{125}I-*HP2* in BALB/C nu/nu mice bearing SKOV-3 xenografts at 1 h p.i. $Z_{HER2:342}$-SR-*HP1* was pre-injected 4 h prior to ^{125}I-*HP2* injection. Data are presented as an average %ID/g with standard deviation for 5 mice.

Injected dose of $Z_{HER2:342}$-SR-*HP1* (µg)	0	5	30	100	5
Injected dose of ^{125}I-*HP2* (µg)	1	1	1	1	5
Uptake, %ID/g					
Blood	0.8±0.2	1.4±0.9	2.1±0.9	2.1±0.5	1.0±0.1
Lung	0.7±0.1	1.2±0.6	2.2±0.7	3.2±0.9	1.01±0.06
Liver	0.44±0.06	0.6±0.2	0.9±0.3	1.0±0.3	0.45±0.03
Spleen	0.35±0.08	0.6±0.2	0.9±0.4	1.0±0.2	0.53±0.06
Kidney	1.8±0.4	2.5±1.3	6.3±3.2	5.6±1.2	10.1±0.5[b]
Tumor	0.3±0.1[a]	17±6	18±8	19±8	3.8±0.3[b]
Muscle	0.19±0.06	0.6±0.5	0.4±0.2	0.6±0.3	0.29±0.09
Bones	0.23±0.08	0.5±0.4	0.5±0.3	0.5±0.3	0.4±0.1
Tumor-to-organ ratio					
Blood	0.41±0.04[a]	10±5	8±1	9±3	4±0.6[b]
Lung	0.48±0.09[a]	13±4	8±1	6±2	3.8±0.4[b]
Liver	0.7±0.1[a]	20±7	19±5	19±5	8.5±0.9[b]
Spleen	0.9±0.2[a]	24±9	19±2	19±6	7±1[b]
Kidney	0.17±0.02[a]	6.6±3	2.9±0.6	3.3±0.9	0.38±0.01[b]
Muscle	1.7±0.4[a]	35±19	41±6	30±17	14±5
Bone	1.4±0.3[a]	32±12	32±1	53±36	11±4[b]

[a] significant difference ($p<0.05$) between values for uptake with and without pre-injection of $Z_{HER2:342}$-SR-*HP1*;
[b] significant difference ($p<0.05$) between groups injected with 1 and 5 µg of ^{125}I-*HP2*;

Table 2. In vivo specificity of ^{111}In-*HP2* in BALB/C nu/nu mice bearing SKOV-3 xenografts at 1 h p.i. in the presence and absence of $Z_{HER2:342}$-SR-*HP1*; one group of mice were pre-injected with 100 µg of $Z_{HER2:342}$-SR-*HP1* 4 h prior to injection of ^{111}In-*HP2*. Data are presented as an average %ID/g with standard deviation for 5 mice.

Injected $Z_{HER2:342}$-SR-*HP1* dose (µg)	0	100
Injected dose of ^{111}In-*HP2* (µg)	1	1
Uptake, %ID/g		
Blood	0.7±0.3	0.4±0.3
Lung	0.8±0.3	0.9±0.2
Liver	0.5±0.3	0.30±0.04
Spleen	0.24±0.05	0.27±0.06
Kidney	10±1	12±2
Tumor	0.3±0.1	19±2*
Muscle	0.2±0.01	0.17±0.07
Bones	0.21±0.06	0.2±0.1
Tumor-to-organ ratio		
Blood	0.53±0.08	54±19*
Lung	0.44±0.03	23±6*
Liver	0.8±0.2	62±9*
Spleen	1.2±0.1	72±17*
Kidney	0.03±0.01	1.8±0.3*
Muscle	2.3±0.5	123±38*
Bones	1.7±0.2	118±63*

* significant difference ($p<0.05$) between groups.

A comparison of the biodistribution of ^{111}In-*HP2* and ^{125}I-*HP2* (both 1 μg, 1 h p.i.) in SKOV-3 xenograft-bearing mice after pre-injection of $Z_{HER2:342}$-SR-*HP1* (100 μg) is presented in Table S2. There was no significant difference in tumor uptake. The kidney uptake of ^{111}In-*HP2* exceeded kidney uptake of ^{125}I-*HP2* 2-fold. However, the concentration of radioactivity in other organs was significantly higher for ^{125}I-*HP2* than that of ^{111}In-*HP2* at 1 h p.i. Consequently, ^{111}In-*HP2* provided significantly higher tumor-to-blood, tumor-to-lung, tumor-to-liver, tumor-to-bone, and tumor-to-muscle ratios than ^{125}I-*HP2* ($p<0.05$) (Table S3).

Imaging

The results of the imaging experiment are presented in Figure 5. Injection of ^{111}In-*HP2* after pre-injection of $Z_{HER2:342}$-SR-*HP1* resulted in clear high-contrast visualization of SKOV-3 xenografts (Figure 5, group A). In agreement with ex vivo measurements, the tumor uptake exceeded the uptake in any other tissue type. Tumors were not visualized when ^{111}In-*HP2* was injected without pre-injection of $Z_{HER2:342}$-SR-*HP1* (Figure 5, group B). The reference ^{111}In-labeled DOTA-$Z_{HER2:K58}$ Affibody molecules also provided clear imaging of tumors (Figure 5, group C), but the renal uptake was much higher than the tumor uptake.

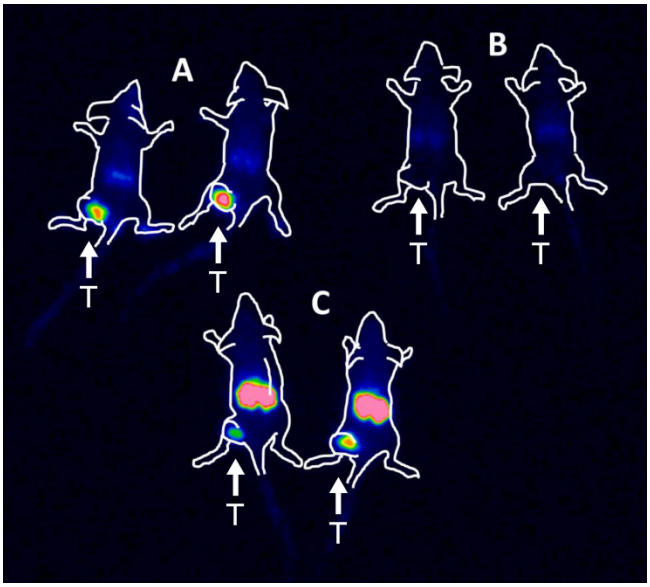

Figure 5. Gamma-camera imaging of HER2 expression in SKOV-3 xenografts using radiolabeled ^{111}In-*HP2* and ^{111}In-DOTA-$Z_{HER2:K58}$ Affibody molecules. All animals were injected with 650 kBq of a radiolabeled compound 1 h before image acquisition. A single image of all animals simultaneously was acquired. Animals were pre-injected with 100 μg $Z_{HER2:342}$-SR-*HP1* 4 h prior to injection of 1 μg ^{111}In-*HP2* (A). ^{111}In-*HP2* was injected without pre-injection of $Z_{HER2:342}$-SR-*HP1* (B). Animals were injected with 2 μg ^{111}In-DOTA-$Z_{HER2:K58}$ (650 kBq) (C).

Discussion

Affibody molecule-based, PNA-mediated pretargeting might be a powerful tool for improving the delivery of radionuclides to tumors. However, there are multiple possible pitfalls with this strategy. For example, Affibody molecules and PNA might create mutual sterical hindrances for binding to a tumor-associated molecular target and a secondary hybridization probe, respectively. The Affibody-PNA chimera might bind nonspecifically to cells or blood proteins, or might be internalized by target cells too rapidly. All these phenomena would compromise the intended accumulation of radionuclides in tumors. Our study shows that this is not the case using our design of hybridization probes.

The ^{111}In-$Z_{HER2:342}$-SR-*HP1* chimera retained the capacity to bind specifically to HER2-expressing living cells (Figure 2 A and B), with a very high affinity determined for the binding to SKOV-3 cells (K_D = 6±2 pM). The internalization of ^{111}In-$Z_{HER2:342}$-SR-*HP1* was slow (ca. 10% at 4 h) in both cancer cell lines tested (Figure 3 A and B), which is a precondition for a successful pretargeting. The binding of ^{125}I-/^{111}In-labeled *HP2* to cancer cells in vitro was very low without $Z_{HER2:342}$-SR-*HP1* pre-treatment (Figures 3 C, D, E and F). In vitro saturation experiments also demonstrated that *HP2* binding was mediated by PNA-PNA hybridization and dependent on the binding of $Z_{HER2:342}$-SR-*HP1* to HER2 cells (Figures 3 C, D, E and F). Binding of radiolabeled *HP2* to $Z_{HER2:342}$-SR-*HP1* pre-treated HER2-expressing cells was described by two apparent dissociation constants: a predominant subnanomolar (293±112 and 336±13 pM, for ^{125}I-*HP2* and ^{111}In-*HP2*, respectively) and a low nanomolar (12.8±6 and 15±5 nM, ^{125}I-*HP2* and ^{111}In-*HP2*, respectively). Both interactions had the same association rate but differed in the dissociation rate (Figures S5 and S6). Interpretation of the affinity pattern is difficult, as the system involves multiple interactions (interactions of receptors of HER family on cells, an interaction of $Z_{HER2:342}$-SR-*HP1* with HER2, an interaction of radiolabeled *HP2* with $Z_{HER2:342}$-SR-*HP1*, and interaction of $Z_{HER2:342}$-SR-*HP1:HP2* complex with HER2). We can observe only binding and dissociation of *HP2*. Some speculation might be based on the facts that affinity of HER-family receptors to their ligands depends on homo-and heterodimerization of receptors (25), and that $Z_{HER2:342}$-SR-*HP1* interaction with HER2-expressing cells has a single dissociation constant. We may hypothesize that homo-and/or heterodimerization of HER2 influences binding of $Z_{HER2:342}$-SR-*HP1:HP2* and results in conformations determining somewhat weaker binding. However, it is difficult to test this hypothesis experimentally. The use of radiometal label for *HP2* provided better reten-

tion of radioactivity (81.2 ± 0.8% and 78.9 ± 0.3% at 24 h for BT474 and SKOV3, respectively) than radioiodine (40.2 ± 0.4% and 49 ± 1 % at 24 h for BT474 and SKOV3, respectively) presumably due to residualizing properties of ^{111}In.

Importantly, the blood clearance of $Z_{HER2:342}$-SR-*HP1* was rapid. The concentration of the blood-born activity was 0.16±0.02 %ID/g in NMRI mice at 4 h (Table S1) or 0.14±0.05 %ID/g in tumor-bearing BALB/C nu/nu mice at 5 h after injection of ^{111}In-$Z_{HER2:342}$-SR-*HP1*. For comparison, the blood concentration in BALB/C nu/nu mice at 4 h after injection of three ^{111}In-labeled $Z_{HER2:342}$ derivatives, ABY-25, DOTA-$Z_{HER2:2395}$-C and synthetic DOTA-$Z_{HER2:342\text{-}pep2}$ was 0.21 ± 0.03, 0.19 ± 0.05 and 0.11 ± 0.03 %ID/g, respectively (30). Thus, the clearance of *HP1*-conjugated $Z_{HER2:342}$was as quick as clearance of non-conjugated $Z_{HER2:342}$, and binding of $Z_{HER2:342}$-SR-*HP1* to blood components did not influence the blood clearance rate.

Further in vivo studies confirmed our hypotheses. The binding of ^{111}In-$Z_{HER2:342}$-SR-*HP1* to HER2-expressing SKOV-3 xenografts was HER2-specific (Figure 4 A). The accumulation of both ^{125}I- and ^{111}In-labeled *HP2* in tumors was shown to be dependent on pretargeting, and without $Z_{HER2:342}$-SR-*HP1* pre-injection the tumor uptake was very low (Tables 1 and 2, Figure 5). Affibody-based PNA-mediated pretargeting can thus provide higher accumulation of radiometals in tumors in comparison with kidneys (Table 2). The use of radioiodinated and radiometal-labeled *HP2* provided equal uptake of radioactivity in tumors (19±8 %ID/g and 18.5±1.5 %ID/g, for ^{125}I-*HP2* and ^{111}In-*HP2*, respectively) at 1 h after injection (Table S2). At this time point, the renal uptake was significantly higher for ^{111}In-*HP2*, but radiometal-labeled *HP2* provided significantly lower uptake in blood, lung, liver, spleen and muscle. Such pattern might be explained by difference in retention of radiometabolites in the catabolic sites, especially kidneys. We may expect that both ^{125}I-*HP2* and ^{111}In-*HP2* are reabsorbed in kidneys to the same extent. However, the residualizing radiometal label remains trapped in kidneys after proteolytic degradation, while "leaky" metabolites of non-residualizing radioiodine label returned to blood circulation. The results of in vivo stability test show much higher fraction of low-molecular-weight catabolites in blood for ^{125}I-*HP2* than for^{111}In-*HP2*, which supports this reasoning.

Earlier, we have evaluated other approaches to radionuclide therapy using Affibody molecules. The slow internalization of Affibody molecules by cancer cells, but rapid internalization in kidney, indicated that the use of non-residualizing labels is possible. This results in rapid excretion of radiometabolites from kidneys, but long retention of radiolabeled Affibody molecules on the surface of cancer cells. In fact, we have shown that the use of non-residualizing labels, such as ^{131}I-*para*-iodo-benzoate (31) or ^{188}Re-GGGC (32), provide higher uptake of radioactivity in tumors than in kidneys. However, the high energy of the beta-particles emitted by ^{188}Re makes it suitable only for treatment of bulky, non-operable tumors. The medium-energy beta particles emitted by ^{131}I are more suitable for eradication of small tumors, but the high abundance, high-energy gamma decay of ^{131}I indiscriminately irradiates the patient's whole body. In contrast, the versatile DOTA chelator in *HP2* enables labeling this probe with the alpha-emitting radiometals $^{212/213}$Bi and ^{227}Th for treatment of micro metastases, the low-energy beta emitter ^{177}Lu for small tumors, and the high-energy beta emitter ^{90}Y for bulky lesions (33–34). This chelator can also be labeled with ^{111}In and ^{68}Ga for theranostics imaging.

A major advantage of pretargeting in comparison with conventional RIT is the rapid clearance of radiolabeled *HP2* from blood and the low accumulation in bones, which reduces exposure of radiosensitive bone marrow. We can foresee some potential advantages in comparison with antibody-based pretargeting methods. The major one is the rapid clearance of $Z_{HER2:342}$-SR-*HP1* from blood, which makes an additional injection of a clearing agent unnecessary. In addition, Affibody molecules can be cost-efficiently produced in high yields in prokaryotes, and PNA-based hybridization probes can be synthesized with relative ease using standard peptide synthesis techniques. This would appreciably reduce the costs of the agents in the case of clinical translation.

In conclusion, the Affibody-based PNA-mediated pretargeting is feasible and provides higher accumulation of radionuclides in tumors than in kidneys.

Supplementary Material

Supplementary data, figures and tables.
http://www.thno.org/v06p0093s1.pdf

Acknowledgement

This research was financially supported by grants from the Swedish Cancer Society (grant 2012/354) and the Swedish Research Council (grants 521-2012-2228 and 621-2013-5135).

Competing Interests

The authors have declared that no competing interest exists.

References

1. Milenic DE, Brady ED, Brechbiel MW. Antibody-targeted radiation cancer therapy. Nat Rev Drug Discov. 2004; 3: 488–99.
2. Pouget JP, Navarro-Teulon I, Bardiès M, Chouin N, Cartron G, Pèlegrin A, Azria D. Clinical radioimmunotherapy--the role of radiobiology. Nat Rev Clin Oncol. 2011; 8: 720–34.
3. Hnatowich DJ, Virzi F, Rusckowski M. Investigations of avidin and biotin for imaging applications. J Nucl Med. 1987; 28: 1294–302.
4. Paganelli G, Malcoviti M, Fazio F. Monoclonal antibody pretargeting techniques for tumor localization: the avidin-biotin system. Nucl Med Commun 1991; 12: 211–234.
5. Rusckowski M, Fogarasi M, Fritz B, Hnatowich DJ. Effect of endogenous biotin on the applications of streptavidin and biotin in mice. Nucl Med Biol 1997; 24: 263–268.
6. Sharkey RM, Karacay H, Cardillo TM, Chang CH, McBride WJ, Rossi EA, Horak ID, Goldenberg DM. Improving the Delivery of Radionuclides for Imaging and Therapy of Cancer Using Pretargeting Methods. Clin Cancer Res. 2005; 11: 71097121.
7. Kuijpers WH, Bos ES, Kaspersen FM, Veeneman GH, van Boeckel CA. Specific recognition of antibody-oligonucleotide conjugates by radiolabeled antisense nucleotides: a novel approach for two-step radioimmunotherapy of cancer. Bioconjug Chem. 1993; 4: 94–102.
8. Mardirossian G, Lei K, Rusckowski M, Chang F, Qu T, Egholm M, Hnatowich DJ. In vivo hybridization of technetium-99m-labeled peptide nucleic acid (PNA). J Nucl Med. 1997; 38: 907–13.
9. Liu G, Mang'era K, Liu N, Gupta S, Rusckowski M, Hnatowich DJ. Tumor pretargeting in mice using (99m)Tc-labeled morpholino, a DNA analog. J Nucl Med. 2002; 43: 384–91.
10. van de Watering FC, Rijpkema M, Robillard M, Oyen WJ, Boerman OC. Pretargeted imaging and radioimmunotherapy of cancer using antibodies and bioorthogonal chemistry. Front Med (Lausanne). 2014; 1: 44.
11. Löfblom J, Feldwisch J, Tolmachev V, Carlsson J, Ståhl S, Frejd FY. Affibody molecules: engineered proteins for therapeutic, diagnostic and biotechnological applications. FEBS letters. 2010; 584: 2678–80.
12. Ahlgren S, Tolmachev V. Radionuclide molecular imaging using Affibody molecules. Curr Pharm Biotechnol. 2010; 11: 581–9.
13. Sörensen J, Sandberg D, Sandström M, Wennborg A, Feldwisch J, Tolmachev V, et al. First-in-human molecular imaging of HER2 expression in breast cancer metastases using the 111In-ABY-025 affibody molecule. J Nucl Med. 2014; 55: 730–5.
14. Feldwisch J, Tolmachev V. Engineering of affibody molecules for therapy and diagnostics. Methods Mol Biol. 2012; 899: 103–26.
15. Egholm M, Buchardt O, Christensen L, Behrens C, Freier SM, Driver DA, Berg RH, Kim SK, Norden B, Nielsen PE. PNA hybridizes to complementary oligonucleotides obeying the Watson-Crick hydrogen-bonding rules. Nature. 1993; 365: 566–8.
16. Boffa LC, Menichini P, Bolognesi C, Cutrona G, Roncella S, Damonte GL, Millo E, Mariani MR, Matis S, Russo D, Ciliutti P, Ferrarini M. Lack of mutagenicity and clastogenicity of Emu-NLS targeted to a regulatory sequence of the translocated c-myc oncogene in Burkitt's lymphoma. Mutat Res. 2007; 628: 129–37.
17. Cutrona G, Boffa LC, Mariani MR, Matis S, Damonte G, Millo E, Roncella S, Ferrarini M. The peptide nucleic acid targeted to a regulatory sequence of the translocated c-myc oncogene in Burkitt's lymphoma lacks immunogenicity: follow-up characterization of PNAEmu-NLS. Oligonucleotides. 2007; 17: 146–50.
18. Upadhyay A, Ponzio NM, Pandey VN. Immunological response to peptide nucleic acid and its peptide conjugate targeted to transactivation response (TAR) region of HIV-1 RNA genome. Oligonucleotides. 2008; 18: 329–35.
19. Wang Y, Chang F, Zhang Y, Liu N, Liu G, Gupta S, Rusckowski M, Hnatowich DJ. Pretargeting with amplification using polymeric peptide nucleic acid. Bioconjug Chem. 2001; 12: 807–16.
20. Rusckowski M, Qu T, Chang F, Hnatowich DJ. Pretargeting using peptide nucleic acid. Cancer. 1997; 80: 2699–705.
21. Westerlund K, Honarvar H, Tolmachev V, Eriksson Karlström A. Design, preparation and characterization of PNA-based hybridization probes for Affibody molecule-mediated pretargeting. Bioconjug Chem. 2015; 26: 1724–36.
22. Tolmachev V, Tran TA, Rosik D, Sjöberg A, Abrahmsén L, Orlova A. Tumor targeting using affibody molecules: interplay of affinity, target expression level, and binding site composition. J Nucl Med. 2012; 53: 953–60.
23. Lundberg E, Höidén-Guthenberg I, Larsson B, Uhlén M, Gräslund T. Site-specifically conjugated anti-HER2 Affibody molecules as one-step reagents for target expression analyses on cells and xenograft samples. J Immunol Methods. 2007; 319: 53–63.
24. Wållberg H, Orlova A. Slow internalization of anti-HER2 synthetic affibody monomer 111In-DOTA-ZHER2:342-pep2: implications for development of labeled tracers. Cancer Biother Radiopharm.2008; 23: 435–42.
25. Björkelund H, Gedda L, Malmqvist M, Andersson K. Resolving the EGF-EGFR interaction characteristics through a multiple-temperature, multiple-inhibitor, real-time interaction analysis approach. Mol Clin Oncol. 2013; 1: 343–352.
26. Tolmachev V, Malmberg J, Estrada S, Eriksson O, Orlova A. Development of a 124I-labeled version of the anti-PSMA monoclonal antibody capromab for immunoPET staging of prostate cancer: Aspects of labeling chemistry and biodistribution. Int J Oncol. 2014; 44: 1998–2008.
27. Tran T, Engfeldt T, Orlova A, Widström C, Bruskin A, Tolmachev V, Karlström AE. In vivo evaluation of cysteine-based chelators for attachment of 99mTc to tumor-targeting Affibody molecules. Bioconjug Chem. 2007; 18: 549–58.
28. Kramer-Marek G, Shenoy N, Seidel J, Griffiths GL, Choyke P, Capala J. 68Ga-DOTA-affibody molecule for in vivo assessment of HER2/neu expression with PET. Eur J Nucl Med Mol Imaging. 2011; 38: 1967–76.
29. Perols A, Honarvar H, Strand J, Selvaraju R, Orlova A, Karlström AE, Tolmachev V. Influence of DOTA chelator position on biodistribution and targeting properties of (111)In-labeled synthetic anti-HER2 affibody molecules. Bioconjug Chem. 2012; 23: 1661–70.
30. Ahlgren S, Orlova A, Wållberg H, Hansson M, Sandström M, Lewsley R, Wennborg A, Abrahmsén L, Tolmachev V, Feldwisch J. Targeting of HER2-expressing tumors using 111In-ABY-025, a second-generation affibody molecule with a fundamentally reengineered scaffold. J Nucl Med. 2010; 51: 1131–8.
31. Tolmachev V, Mume E, Sjöberg S, Frejd FY, Orlova A. Influence of valency and labelling chemistry on in vivo targeting using radioiodinated HER2-binding Affibody molecules. Eur J Nucl Med Mol Imaging. 2009; 36: 692–701.
32. Altai M, Wållberg H, Honarvar H, Strand J, Orlova A, Varasteh Z, Sandström M, Löfblom J, Larsson E, Strand SE, Lubberink M, Ståhl S, Tolmachev V. 188Re-ZHER2:V2, a promising affibody-based targeting agent against HER2-expressing tumors: preclinical assessment. J Nucl Med. 2014; 55: 1842–8.
33. Price EW, Orvig C. Matching chelators to radiometals for radiopharmaceuticals. Chem Soc Rev. 2014; 43: 260–90.
34. Heyerdahl H, Krogh C, Borrebæk J, Larsen Å, Dahle J. Treatment of HER2-expressing breast cancer and ovarian cancer cells with alpha particle-emitting 227Th-trastuzumab. Int J Radiat Oncol Biol Phys. 2011; 79: 563–70.